Am J Cancer Res 2023;13(1):276-292
www.ajcr.us /ISSN:2156-6976/ajcr0146392

Original Article

DOT1L promotes cell proliferation and invasion by epigenetically regulating STAT5B in renal cell carcinoma

Yanguang Hou[1,2], Shiyu Huang[1,2], Jiachen Liu[1,2], Lei Wang[1], Yan Yuan[1], Hao Liu[1], Xiaodong Weng[1], Zhiyuan Chen[1], Juncheng Hu[1,2], Xiuheng Liu[1]

[1]Department of Urology, Renmin Hospital of Wuhan University, Wuhan 430060, Hubei, PR China; [2]Wuhan University Institute of Urologic Disease, Renmin Hospital of Wuhan University, Wuhan 430060, Hubei, PR China

Received September 8, 2022; Accepted December 14, 2022; Epub January 15, 2023; Published January 30, 2023

Abstract: DOT1L, the only histone H3 lysine 79 methyltransferase, has a prominent effect on promoting the progression of various malignancies, yet the functional contribution of DOT1L to renal cell carcinoma (RCC) progression remains unclear. DOT1L is overexpressed in RCC and linked to poor clinical outcomes. Chemical (SGC0946) or genetic suppression of DOT1L attenuates the growth and invasion of renal cancer cells and results in S-phase arrest. STAT5B expression was suppressed after DOT1L knockdown, and STAT5B overexpression rescued the DOT1L silencing-induced decrease in cell proliferation. DOT1L was found to epigenetically promote the transcription of STAT5B via H3K79me2, and CDK6 acted as a downstream effector of STAT5B to mediate cell cycle arrest. Our study confirmed that DOT1L promotes STAT5B expression in a histone methyltransferase-dependent manner. Downregulation of DOT1L inhibited RCC proliferation and invasion. Thus, targeting DOT1L might be a potential therapeutic intervention for RCC.

Keywords: Renal cell carcinoma, histone methylation, DOT1L, STAT5B, CDK6

Introduction

Renal cell cancer (RCC) is the major subtype of kidney cancer, accounting for more than 90% of renal malignancies [1]; it has a 5-year survival rate of 76% and accounts for approximately 2% of global cancer deaths. Clear cell RCC (ccRCC) is the most common pathological subtype of RCC. Mutations in the von Hippel-Lindau (VHL) gene, as well as tumor suppressor genes, including SET domain-containing protein 2 (SETD2), BRCA1-associated protein 1 (BAP1), and Protein polybromo-1 (PBRM1), are frequently found in ccRCC [2]. Generally, the prognosis of ccRCC is poorer than that of papillary and chromophobe RCC due to its high vascular invasion, metastasis and mortality rates [3]. Currently, standard surgical resection techniques are widely performed to effectively treat localized tumors. However, approximately one-third of patients with local RCC experience tumor recurrence after surgery [4]. Therefore, it is very important to explore new, more reliable and more efficient biomarkers to reveal the cellular mechanism underlying tumor progression and metastasis.

Recently, researchers have increasingly focused on histone modifications, owing to their intimate involvement in gene expression, metabolism regulation, and cancer progression [5, 6]. Disruptor of telomeric silencing-1-like (DOT1L, or KMT4) is the only histone methyltransferase that can catalyze H3K79 methylation. H3K79 methylation is related to the DNA damage response, cell cycle, and transcriptional elongation by RNA polymerase II [7]. Recent research has proven that DOT1L is crucial in many malignancies, including leukemia [8, 9], breast cancer [10], ovarian cancer [11], colorectal cancer [12], prostate cancer [13] and gastric cancer [14]. Additionally, in patients with ccRCC, higher DOT1L expression was linked to worse overall survival (OS) and recurrence-free survival (RFS) prognoses [15].

To date, DOT1L and its potential role in RCC have not been fully investigated. Here, we

Table 1. The sequences of shRNA for DOT1L knockdown

Description	Sequences
DOT1L sh1-F	CCGGTCGCCAACACGAGTGTTATATCTCGAGATATAACACTCGTGTTGGCGATTTTTG
DOT1L sh1-R	AATTCAAAAATCGCCAACACGAGTGTTATATCTCGAGATATAACACTCGTGTTGGCGA
DOT1L sh2-F	CCGGCACGTTGAACAAGTGCATTTACTCGAGTAAATGCACTTGTTCAACGTGTTTTTG
DOT1L sh2-R	AATTCAAAAACACGTTGAACAAGTGCATTTACTCGAGTAAATGCACTTGTTCAACGTG

Table 2. The sequences of prime for overexpression of STAT5B

Description	Sequences
STAT5B primer-F	CCGGAATTCATGGCTGTGTGGAT
STAT5B primer-R	GGGGTACCTCACGATTGTGCG

aimed to explore the expression of DOT1L and its prognostic value, to analyze its association with RCC progression and invasion, and to identify its molecular mechanism in RCC. Our study provided evidence indicating that targeting DOT1L might be a therapeutic intervention for RCC.

Materials and methods

Clinical data and samples

Clinical data were downloaded from several online databases, including Gene Expression Profiling Interactive Analysis (GEPIA), Gene Expression Omnibus (GEO) database, and UCSC Xena. A total of 34 tissue samples, concluding 12 pairs of cancer tissues and adjacent tissues and 10 tumor tissues (T = 22, N = 12), were included in our study. These samples were obtained from ccRCC patients who underwent surgery in the Department of Urology, Renmin Hospital of Wuhan University, between January 2020 and March 2022. The tissue samples were obtained from the patients after informed consent was provided.

General reagents and antibodies

SGC0946 (#HY-15650, HPLC≥99.68%) was purchased from MedChemExpress (Shanghai, China). Matrigel (#356234) was produced by BD Biosciences (San Jose, CA, USA). Lipo293™ Transfection Reagent (#C0521), blasticidin (#ST018-10 mg), and G418 (#ST081-1 ml) were purchased from Beyotime Biotechnology (Shanghai, China). Antibodies against DOT1L (#ab239358), H3K79me2 (#ab3594), MMP2 (#ab92536), MMP9 (#ab228402), B-cell lymphoma-2 (Bcl2; #ab182858), CDK6 (#ab124821), P21 (#ab109520), and STAT5B (ab178941) were purchased from Abcam (Cambridge, MA). Antibodies against cyclin A2 (CCNA2; #91500), Bcl2-associated X protein (Bax; #5023), and phospho-STAT5 (Tyr694) (#4322) were purchased from Cell Signaling Technology (Massachusetts, USA). The housekeeping proteins GAPDH (#10494-1-AP) and H3 (#17168-1-AP) were obtained from Proteintech Group (Hubei, China).

Cell culture and inhibitors

RCC cell lines (786-O and A498) were purchased from the China Center for Type Culture Collection (CCTCC) and cultured as recommended in RPMI-1640 medium containing 10% FBS in 5% CO_2 at 37°C. The human renal epithelial cell line (HK-2) and HEK 293T cells were grown in DMEM containing 10% FBS. Dimethyl sulfoxide (DMSO) was used to dissolve SGC0946 as a 10 mM stock solution. The working concentrations were 0 (or DMSO), 1, 2, 5, and 10 μM.

Plasmids and lentiviruses

For genetic suppression of DOT1L expression, two shRNAs were individually inserted in the pLKO.1 lentiviral vector between the Age I and EcoR I restriction sites. The two shRNAs were synthesized by Sangon Biotech (Shanghai, China). The shRNA sequences are listed in **Table 1**. The pLKO.1, psPAX2, pMD2.G (Addgene, Beijing, China) plasmids were cotransfected into HEK 293T cells, and the conditioned medium (CM) was collected after 48 h and 72 h. Another shRNA that did not target any gene was used as a control construct. Then, the conditioned medium was added to 786-O cells, and blasticidin was used to select stably transfected 786-O cells.

For overexpression of the STAT5B gene, the CDS was inserted into the pEGFP-N1 vector between the EcoR I and Kpn I restriction sites. The primer sequences used for the STAT3B overexpression construct are listed in **Table 2**.

Table 3. The qPCR primers of different genes

Description	Sequences
GAPDH-F	GTCTCCTCTGACTTCAACAGCG
GAPDH-R	ACCACCCTGTTGCTGTAGCCAA
DOT1L-F	GCTGCCGGTCTACGATAAACA
DOT1L-R	AGCTTGAGATCCGGGATTTCT
CCNA1-F	GCCTGGCAAACTATACTGTG
CCNA1-R	CTCCATGAGGGACACACACA
CCNA2-F	CCTCCTTGGAAAGCAAACAGT
CCNA2-R	CAGGGCATCTTCACGCTCTAT
CCNB1-F	CTTGCAGTAAATGATGTGGATG
CCNB1-R	GTGACTTCCCGACCCAGTAG
CCNB2-F	CCGACGGTGTCCAGTGATTT
CCNB2-R	TGTTGTTTTGGTGGGTTGAACT
CCND1-F	TGCTGGTTTTCTACCCAACG
CCND1-R	AGTGCTTGGAAATGGAATGG
CCND2-F	TTTAAGTTTGCCATGTACCCAC
CCND2-R	ACGTCTGTGTTGGTGATCTTAG
CCNE2-F	GATGGAACTCATTATATTAAAGGCTT
CCNE2-R	AGGAGCATCTTTAAGAGCATCAACTT
CDK2-F	GGCATTCCTCTTCCCCTCA
CDK2-R	GCTCTGGCTAGTCCAAAGTCTG
CDK4-F	GTCTATGGTCGGGCCCTCT
CDK4-R	CCATAGGCACCGACACCAAT
CDK6-F	GGATAAAGTTCCAGAGCCTGGAG
CDK6-R	GCGATGCACTACTCGGTGTGAA
STAT5B-F	CACAGTTCAGCGTCGGTGGAAA
STAT5B-R	CTGTGGCATTGTTGTCCTGGCT
p21-F	GGCAGACCAGCATGACAGATT
p21-R	GCGGATTAGGGCTTCCTCT
p53-F	TAACAGTTCCTGCATGGGCGGC
p53-R	AGGACAGGCACAAACACGCACC
Rb-F	GCAGTATGCTTCCACCAGGC
Rb-R	AAGGGCTTCGAGGAATGTGAG

The pEGFP-N1-STAT5B vector (oeSTAT5B) or pEGFP-N1 (sham) vector was transfected into 786-O cells with stable DOT1L gene knockdown via sh2 transfection. Then, we used G418 to select the stably transfected cells. To assess the DNA transfection efficiency of 786-O cells after incubation with pEGFP-N1 at the 24 h time point, we observed the intensity of green fluorescent protein under a fluorescence microscope.

Immunohistochemistry

Clinical samples or tumor bodies from the xenograft model in nude mice were paraffin-embedded. Then, the sections were sliced and subjected to immunohistochemical (IHC) analysis. In brief, after deparaffinization and rehydration, tissue sections were subjected to antigen recovery in sodium citrate buffer. After blocking with 5% goat serum at ambient temperature for 1 h, the slides were incubated with an anti-DOT1L polyclonal antibody at 4°C overnight. The sections were then incubated with a secondary antibody conjugated to horseradish peroxidase (1:100; Dako). Hematoxylin was used to restain the slides after the detection step involving incubation with diaminobenzidine for 8 min. Finally, we visualized the sections using a microscope.

Cell counting kit-8 (CCK-8) assay

The CCK-8 assay was carried out following accepted methods (#ZP327-1, Being, China). In brief, 96-well plates were seeded with 3×10^3 cells per well. At the specified predetermined time points, we added CCK-8 solution to each well and incubated the cells for 1 h. The optical density (OD) value at 450 nm (OD450) was evaluated using a microplate reader. Cell proliferation was indicated by the OD450 value.

Real-time quantitative PCR (RT-qPCR)

After total RNA was extracted by TRIzol (Invitrogen, Carlsbad, CA), cDNA was reverse transcribed with the PrimeScript RT Reagent Kit with gDNA Eraser (Cat. #RR047A). RT-qPCR was performed with TB Green®Premix Ex Taq™ II (Cat. #RR820A) in a CFX96 Touch™ Real-Time qPCR Detection System (Bio-Rad Laboratories, USA) or a Roche LightCycler 480-II System. **Table 3** lists the primer sequences employed for qPCR. Relative mRNA expression was normalized to GAPDH expression. Each sample was measured at least three times, and the mRNA levels were quantified using the ΔΔCt method.

Western blot analysis

We used precooled RIPA lysis buffer to lyse and harvest cells. After centrifugation at 12,000×g for 15 min at 4°C, the protein concentrations were measured by a BCA Protein Assay Kit (P0010S), and the proteins were then separated on SDS-PAGE gels with a suitable concentration and electrotransferred from the gel to PVDF membranes (Merck & Co., USA). After

Table 4. The primers of different location in STAT5B promoter

Description	Sequences
STAT5B promoter primer1-F	GTCCTGGCTCACTTTGCAGTTG
STAT5B promoter primer1-R	AAATCTCCACTCTCTAGGCACAG
STAT5B promoter primer2-F	TCAGAGGGCACGTCATTAGC
STAT5B promoter primer2-R	GTCAGGAGGCTAGGAGACCA
STAT5B promoter primer3-F	GGAGAAAGGCAGCTACCACA
STAT5B promoter primer3-R	TGGCCTTCCTGCATGTTCTT
STAT5B promoter primer4-F	ATTACAGGCGCCACCACTC
STAT5B promoter primer4-R	CCCGGCCCTATTTGTTCCTT
STAT5B promoter primer5-F	CCAAAGGGCAGAAACAACCC
STAT5B promoter primer5-R	TGTCCTGTGTGTCAGCACTT
STAT5B promoter primer6-F	CACCCCTGTAGTCCCACCTA
STAT5B promoter primer6-R	TGCGGTCTTTTGTACTTGGC

Table 5. The primers to bind to the CDK6 promoter

Description	Sequences
CDK6 promoter primer-F	GGGGGTACCCCAGTGTAGAAAAGACAC
CDK6 promoter primer-R	TCCCCCGGGTCTGGGGAAGGAGTTACCA

blocking with 5% skim milk, the membranes were incubated with primary antibodies at 4°C overnight. Then, the membranes were immunoblotted using specific HRP-conjugated secondary antibodies, and immunoreactions were detected via an ECL detection system (Chemi-DocTM XRS+, Bio-Rad). The loading controls were GAPDH and H3.

Wound healing assays

Six-well plates were employed for cell culture. A 200 μL pipette tip was used to create artificial wounds by scraping. After the wounds were made, the cells were washed with PBS. Images of the wounded region were acquired at 0 and 24 h. ImageJ was used to estimate the width of the wounds.

Transwell assay

Transwell chambers containing filter membranes were used to conduct invasion assays. Matrigel was applied to the top surface of the filter membrane (Becton Dickinson, USA) and incubated at ambient temperature after drying at 37°C for two hours. Cells were seeded in the upper chamber (5×10^4 cells/well), and cells that invaded the lower surface of the filter were fixed and stained after 24 h. Under a high-magnification light microscope, the cells in 5 randomly selected areas were counted.

Apoptosis and cell cycle analyses

Apoptosis and cell cycle anaylses were conducted using flow cytometry (Backman CytoFlex, USA). Different groups of cells were seeded in 6 cm plates or treated with different GSC0946 concentrations. For the apoptosis assay, cells were resuspended in 500 μl of binding buffer, and then 5 μl of Annexin V-FITC and 10 μl of PI (ZP327-1, Beijing Zomen Biotechnology) were added. The cells were detected using a flow cytometer after being incubated for 10 min at ambient temperature in a dim environment. Viable cells were negative for Annexin V and PI staining. For cell cycle analysis, cells were washed in precooled PBS and incubated in 75% ethanol for at least 24 h. The cells were then incubated with RNase for 1 h at 37°C and stained with PI for 15 min in the dark. Cells were finally detected by flow cytometry and analyzed using FlowJo 10.7.2 software.

ChIP

The ChIP assay was performed according to the instructions provided with the ChIP Assay Kit (P2078, Beyotime Biotechnology). In brief, crosslinking was performed using 1% formaldehyde at ambient temperature for 10 min, and then the reaction was stopped by 0.125 M glycine. The cells (approximately 10^6) were resuspended in 200 μl of SDS lysis buffer. DNA was sonicated into fragments. Then, the cell lysates were immunoprecipitated with specific antibodies (against H3K79me2 or STAT5B) at 4°C overnight and incubated with 60 μl of Protein A+G Agarose/Salmon Sperm DNA for 1 h at 4°C. The precipitates were washed and eluted. Then, 20 μl of 5 M NaCl was added to the mixture to reverse the crosslinking at 65°C for 4 h. The DNA fragments were then resuspended in ddH2O and were finally measured by qPCR (**Table 4**) or agarose gel electrophoresis.

Dual-luciferase reporter assays

The promoter domain of CDK6 (positions -2000-0) was inserted into the pGL3-Basic vector between the KpnI and SmaI restriction sites.

Table 5 contains the CDK6 promoter primer sequences. 786-O cells ($2*10^5$ cells/well) were seeded in 12-well plates. Using Lipofectamine 2000, 1 μg of the CDK6 promoter reporter plasmid and 50 nanograms of the pRL-TK plasmid were cotransfected per well. Luciferase activities were measured with a dual-luciferase reporter assay kit (Promega, E1910) and quantified with a Centro XS LB 960 luminometer (Berthold Technologies) after 48 h, as directed by the manufacturer. For each well, the firefly luciferase activity was normalized to Renilla luciferase activity.

Tumor xenograft model in nude mice

Six-week-old male BALB/c-nu/nu nude mice were purchased from Wuhan SHULAIBAO Biotechnology (Wuhan, China) and maintained in specific pathogen-free conditions. The Laboratory Animal Ethics Committee of Renmin Hospital of Wuhan University approved all animal experiments.

For the proliferation assay, 5×10^6 786-O cells stably transduced with DOT1L-ctrl, DOT1L-sh1 or DOT1L-sh2 were suspended in PBS with 50% Matrigel and injected subcutaneously into the posterior neck region of nude mice (five mice in each group). During the animal experiment period, the major (L) and minor (W) axes of the tumors were measured, and the tumor volumes were calculated once weekly for up to 5 weeks. The formula used to determine the tumor volume (V) (in mm^3) was $V = L\times W^2/2$.

Statistical analyses

Statistical analyses were performed by Student's t test or ANOVA. Correlations were analyzed via Pearson correlation analysis. $P< 0.05$ was considered statistically significant: *P<0.05, **P<0.01, ***P<0.001.

Results

DOT1L is upregulated in ccRCC and correlates with poor prognosis

To investigate the function of DOT1L in RCC, we first analyzed its expression in data downloaded from the GEO database and The Cancer Genome Atlas (TCGA). The DOT1L expression in ccRCC tissues was higher than that in noncancerous samples (**Figure 1A-C**). Next, we performed IHC staining of 34 tissue samples from ccRCC patients to evaluate DOT1L expression in ccRCC. DOT1L expression was also increased in ccRCC tissues compared with normal tissues (**Figure 1D**).

To further explore DOT1L expression in ccRCC, we selected two ccRCC cell lines (786-O and A498) and one normal cell line (HK-2). The DOT1L levels in the ccRCC cell lines were higher than those in the normal kidney cell line, as determined by qPCR and western blotting (**Figure 1E**, **1F**).

To investigate the prognostic value of the DOT1L level in ccRCC, the Kaplan-Meier Plotter database was used to conduct survival analysis, and the results revealed that the OS of patients with high DOT1L expression was significantly worse than that of patients with low DOT1L expression (**Figure 1G**).

DOT1L inhibition suppresses ccRCC cell proliferation and invasion

SGC0946 is a highly potent and selective DOT1L methyltransferase inhibitor [16]. To determine whether DOT1L has a function in the growth of renal cancer cells, we exposed 786-O and A498 cells to several concentrations of SGC0946 for 48 h.

The CCK-8 assay results showed that SGC0946 drastically reduced the survival of renal cancer cells (**Figure 2A**, **2B**). The effect of SGC0946 on apoptosis was evaluated by flow cytometry, and the results indicated that SGC0946 increased the apoptosis rate of 786-O and A498 cells (**Figure 2C**), reduced the protein level of the apoptotic molecule BCL2, and increased the BAX protein level (**Figure 2F**), confirming that DOT1L inhibition promotes the apoptosis of renal cancer cells. These results revealed that DOT1L inhibition decreased 786-O and A498 cell growth in vitro.

We next investigated the migration and invasion of renal cancer cells after treatment with SGC0946. The wound healing assay showed that the wound closure ability was significantly weakened in 786-O and A498 cells treated with SGC0946 compared with DMSO (**Figure 2D**). The Transwell assay showed a significant decrease in the invasion rate of SGC0946-treated 786-O cells compared with DMSO-treated cells (**Figure 2E**). This decrease was possibly associated with downregulation of the

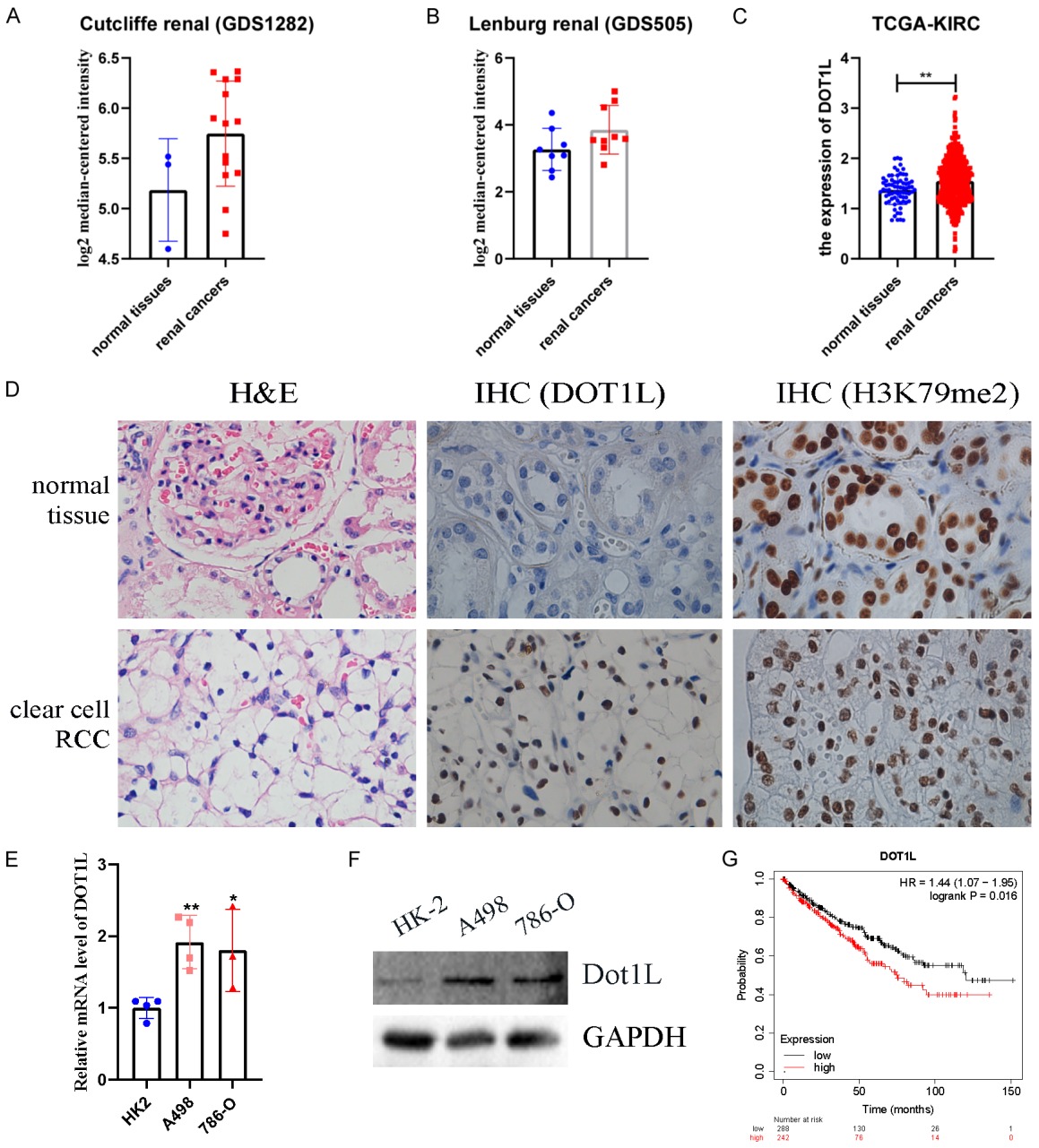

Figure 1. DOT1L expression is elevated in RCC, and high DOT1L expression predicts poor outcomes. A, B. Relative DOT1L expression in normal kidney and ccRCC tissues in the Cutcliffe Renal data set and Lenburg Renal data set from the GEO database. C. Relative DOT1L expression in normal kidney and ccRCC tissues from the TCGA-KIRC data set. D. IHC staining analysis of DOT1L expression in ccRCC (T = 22) samples and normal tissues (N = 12). E. Relative DOT1L mRNA levels in the human kidney cell line HK-2 and two renal cancer cell lines (A498, 786-O) were determined by qPCR. *P<0.05; **P<0.01 compared with HK2 cells. F. The protein expression of DOT1L in the HK-2, 786-O and A498 cell lines was measured by Western blotting. G. Kaplan-Meier analysis of the association between DOT1L expression and OS probability in ccRCC (http://kmplot.com/analysis/index.php?p=service).

invasion markers matrix metalloproteinase 2 (MMP2) and MMP9 (**Figure 2G**). Together, these results revealed that DOT1L inhibitor treatment suppressed the growth and invasion of RCC cells.

DOT1L knockdown suppresses RCC cell proliferation and invasion

To further investigate the function of DOT1L in RCC cells, we used stable lentivirus-mediated

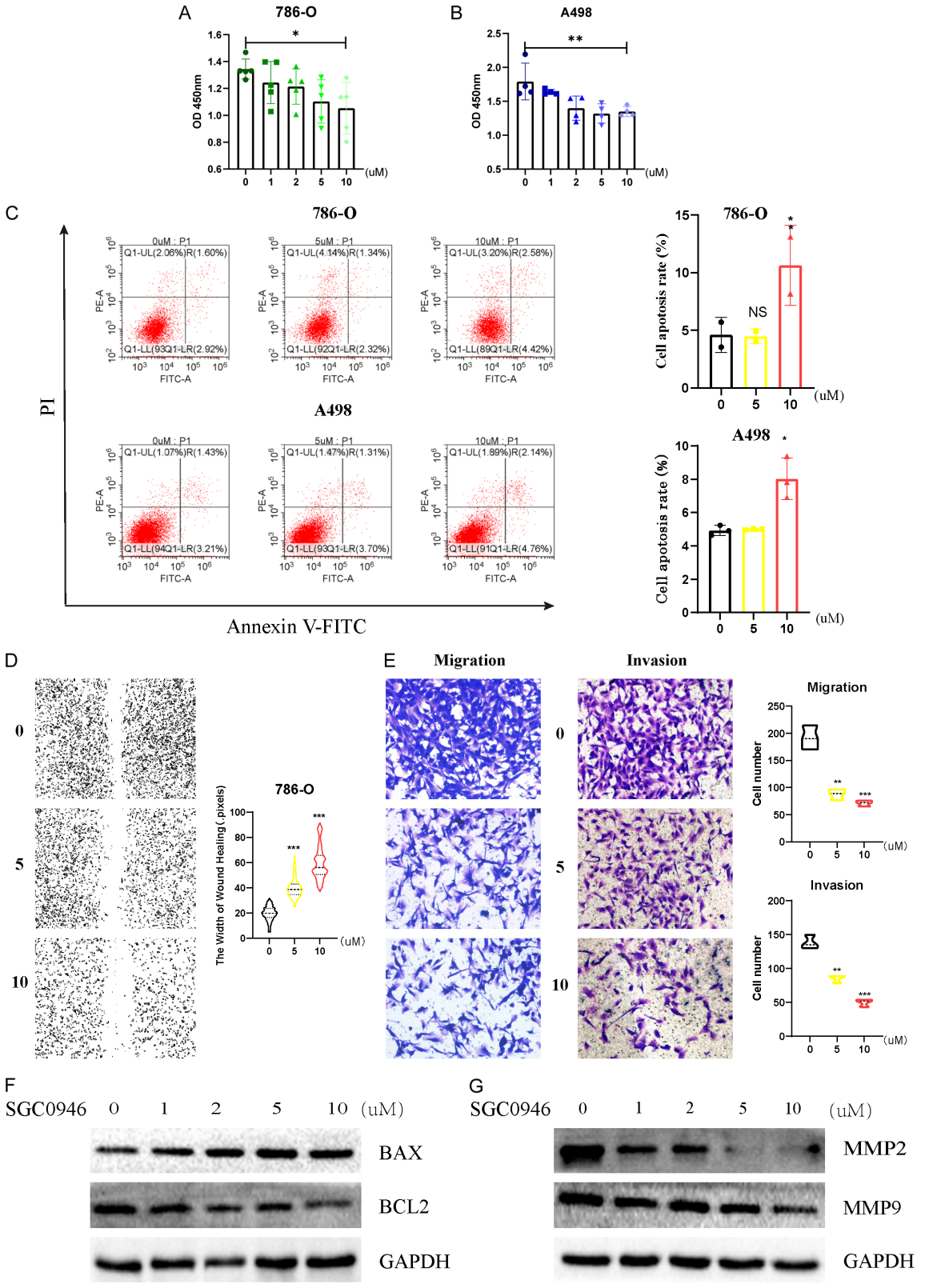

Figure 2. DOT1L inhibition suppresses the proliferation and invasion of ccRCC cells. A, B. Cell growth histogram constructed from CCK8 assay data in 786-O and A498 cells after treatment with 0 μM, 1 μM, 2 μM, 5 μM, or 10 μM SGC0946 for 48 h. C. Apoptosis in 786-O and A498 cells treated with different concentrations of SGC0946 was evaluated by flow cytometry. D. The cell migration ability was evaluated by a wound healing assay in 786-O cells (100×). E. The cell migration and invasion capacities were evaluated by a Transwell assay (100×). F, G. The levels of apoptosis-related proteins and invasion-related proteins were evaluated by Western blotting. *P<0.05; **P<0.01; ***P<0.001 compared with the 0 μM group.

transduction of shRNA to knock down DOT1L in 786-O cells. qPCR and Western blotting verified the successful knockdown of DOT1L by the shRNA lentiviral particles (**Figure 3A**, **3B**). To determine whether DOT1L knockdown can decrease the proliferation of renal cancer cells, a CCK8 assay was performed. Compared with those in the control (ctrl) group, the OD450 values of 786-O cells transfected with shRNAs were significantly decreased ($P<0.05$) (**Figure 3C**). Then, we performed a flow cytometric analysis of apoptosis. The apoptosis rate of shDOT1L cells was increased compared with that of control cells (**Figure 3D**). The level of BCL2 protein was decreased, and that of BAX was increased (**Figure 3B**).

We next investigated the migration and invasion of renal cancer cells after DOT1L knockdown. The wound closure ability was significantly weakened in DOT1L knockdown 786-O cells compared with ctrl cells (**Figure 3E**). The Transwell assay revealed that DOT1L knockdown in 786-O cells significantly inhibited their invasion ability (**Figure 3F**).

Finally, we investigated whether DOT1L knockdown can inhibit renal cancer cell growth in vivo. Subcutaneous implantation of DOT1L-ctrl and DOT1L-sh 786-O cells was performed. On day 35, all mice were analyzed. Representative mice are shown in **Figure 3G**. The tumor volumes in the DOT1L-sh group were noticeably lower than those in the control groups (**Figure 3H**). Immunohistochemical staining validated the relative expression of DOT1L in tumor tissues from the nude mice. DOT1L expression in the DOT1L-sh group was significantly decreased (**Figure 3I**).

Together, our data suggested that DOT1L knockdown suppressed cell proliferation and invasion in RCC.

DOT1L inhibition or knockdown induces S-phase arrest

Given that cell cycle is crucial for cell growth, we then explored the impacts of DOT1L inhibition and knockdown on the cell cycle in renal cancer cells. PI staining followed by flow cytometry showed that the number of 786-O cells in S phase was increased after either knockdown or silencing of DOT1L compared with either the 0 μM group or the control group (**Figure 4A**, **4B**). In addition, the mRNA levels of cell cycle-related mediators such as cyclin A2, cyclin D2 (CCND2), CDK2, CDK4, and CDK6 were drastically decreased after DOT1L knockdown, while the expression of the cell cycle inhibitors p21 and p53 was considerably increased (**Figure 4C**). Moreover, the protein expression levels of CDK6, cyclin A2, and p21 followed the same patterns as the corresponding mRNA levels (**Figure 4D**). These findings demonstrated that DOT1L inhibition and silencing suppressed proliferation by controlling the cell cycle in renal cancer cells.

DOT1L regulates STAT5B in a histone methyltransferase-dependent manner

To explore the universally related genes after DOT1L inhibition, we selected four data sets from different species, different cell lines and different interventions in the GEO database (**Table 6**). Forty-two coexpressed differentially expressed genes (DEGs) were identified by constructing a Venn diagram (**Figure 5A** and **Table 7**). Then, we analyzed DOT1L mRNA expression using data from the TCGA-KIRC cohort. Gene set enrichment analysis (GSEA) revealed that DOT1L was closely linked to the KEGG pathway JAK-STAT SIGNALING (**Figure 5B**). The Janus kinase-signal transducer and activator of transcription (JAK-STAT) signaling pathway is associated with cell immunity, cell division and death, and tumor formation [17]. Moreover, STAT5B was among the 42 overlapping differentially expressed genes. A previous study showed that inhibition of DOT1L, resulting in a reduction in H3K79me2, impairs T-cell antitumor immunity via STAT5B [18]. Therefore, STAT5B may act as a downstream effector of DOT1L to mediate the inhibition of cell proliferation and invasion. Then, we detected the correlation between DOT1L and STAT5B expression in the GEPIA database and found a strong correlation (**Figure 5C**).

By high-throughput techniques, the function of H3K79 methylation in transcriptional regulation was found in prior reports to be to identify particular chromatin modifications on a genome-wide scale [7, 19, 20]. H3K79me2 was found to be significantly more abundant in promoter regions and gene bodies than in other locations in the genome. Therefore, H3K79me2 is the most prominent functional executor of DOT1L-induced H3K79 methylation, and researchers have thus paid more attention to

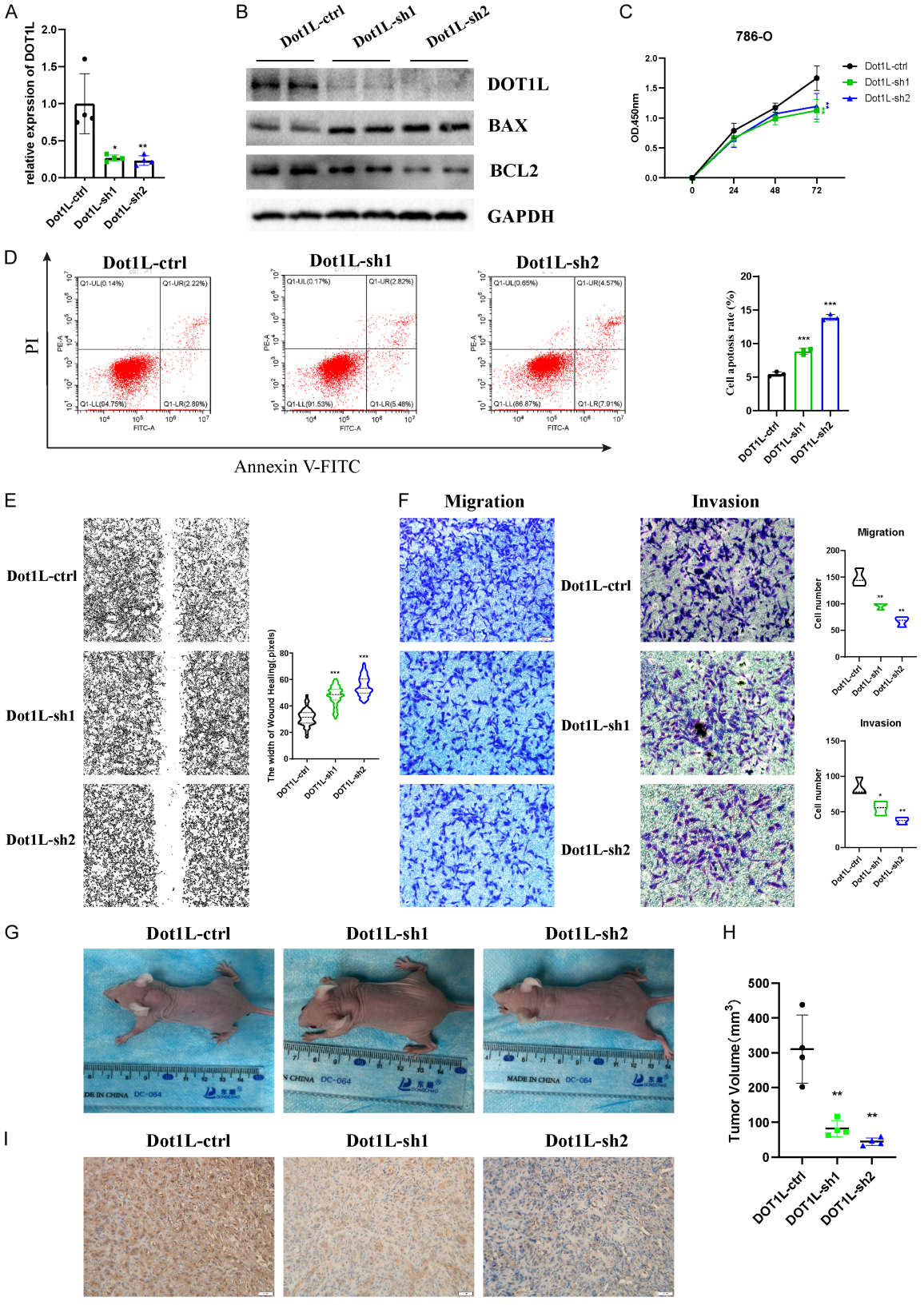

Figure 3. DOT1L silencing reduced the proliferation and invasion of ccRCC cells. A. Relative DOT1L mRNA expression was determined via qPCR in DOT1L knockdown 786-O cells. B. The protein levels of DOT1L, BCL2, and BAX were measured by Western blotting in DOT1L knockdown 786-O cells. C. Cell growth curve constructed from CCK8 assay data in DOT1L knockdown 786-O cells after incubation for 0/24/48/72 h. D. Apoptosis in DOT1L knockdown 786-O cells was evaluated by flow cytometry. E. The cell migration ability was evaluated by a wound healing assay in DOT1L

knockdown 786-0 cells (100×). F. The cell invasion ability was evaluated by a Transwell assay (100×). G. Photos of representative mice from all groups. H. Tumor volumes in each group (n = 4). I. IHC analysis of DOT1L expression in tumor tissues from the nude mice in each group. Scale bar = 50 μm. *P<0.05; **P<0.01; ***P<0.001 compared with the ctrl group.

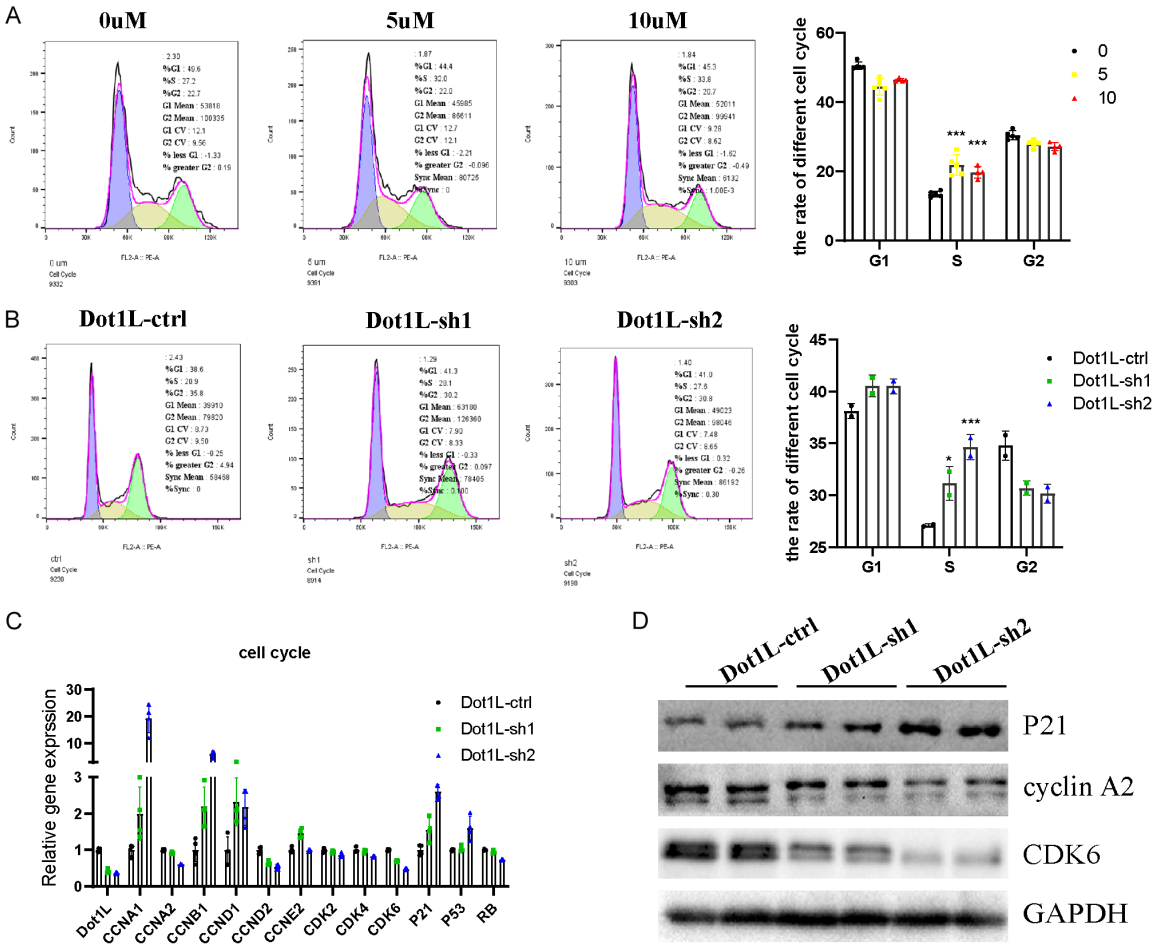

Figure 4. Inhibition or knockdown of DOT1L induces S-phase arrest in 786-0 cells. A. The cell cycle was analyzed by flow cytometry in 786-0 cells treated with SGC0946 (left). Cell cycle data are presented as the means ± SDs (right). B. The cell cycle was analyzed by flow cytometry in 786-0 cells after DOT1L knockdown (left). Cell cycle data are presented as the means ± SDs (right). C. The mRNA levels of cell cycle-related proteins, including cyclin A1, A2, B1, D1, D2, and E2; CDK2, CDK4, and CDK6; and P21, p53, and RB, were measured by qPCR in 786-0 cells after DOT1L knockdown. D. The protein levels of selected cell cycle-related proteins (P21, cyclin A2, and CDK6) were measured by using western blotting in DOT1L knockdown 786-0 cells. *P<0.05; **P<0.01; ***P<0.001 compared with the 0 μM group or control group.

Table 6. The detail information of four GEO Datasets

	Treatment	Cell line	Organism	Contact Name
GSE108694	SGC0946	CD8+ T cells	Homo sapiens	Yuki Kagoya
GSE139070	SGC0946	SU8686	Homo sapiens	Zhiwei Liu
GSE161367	DOT1L knockout	K562	Homo sapiens	Aiwei Wu
GSE150845	DOT1L knockout	CD8+ T cells	Mus musculus	Yingjie Bian

H3K79me2 [18, 21]. We subsequently explored whether DOT1L silencing suppresses proliferation and invasion via STAT5B in renal cancer cells. First, we found that the STAT5B level was

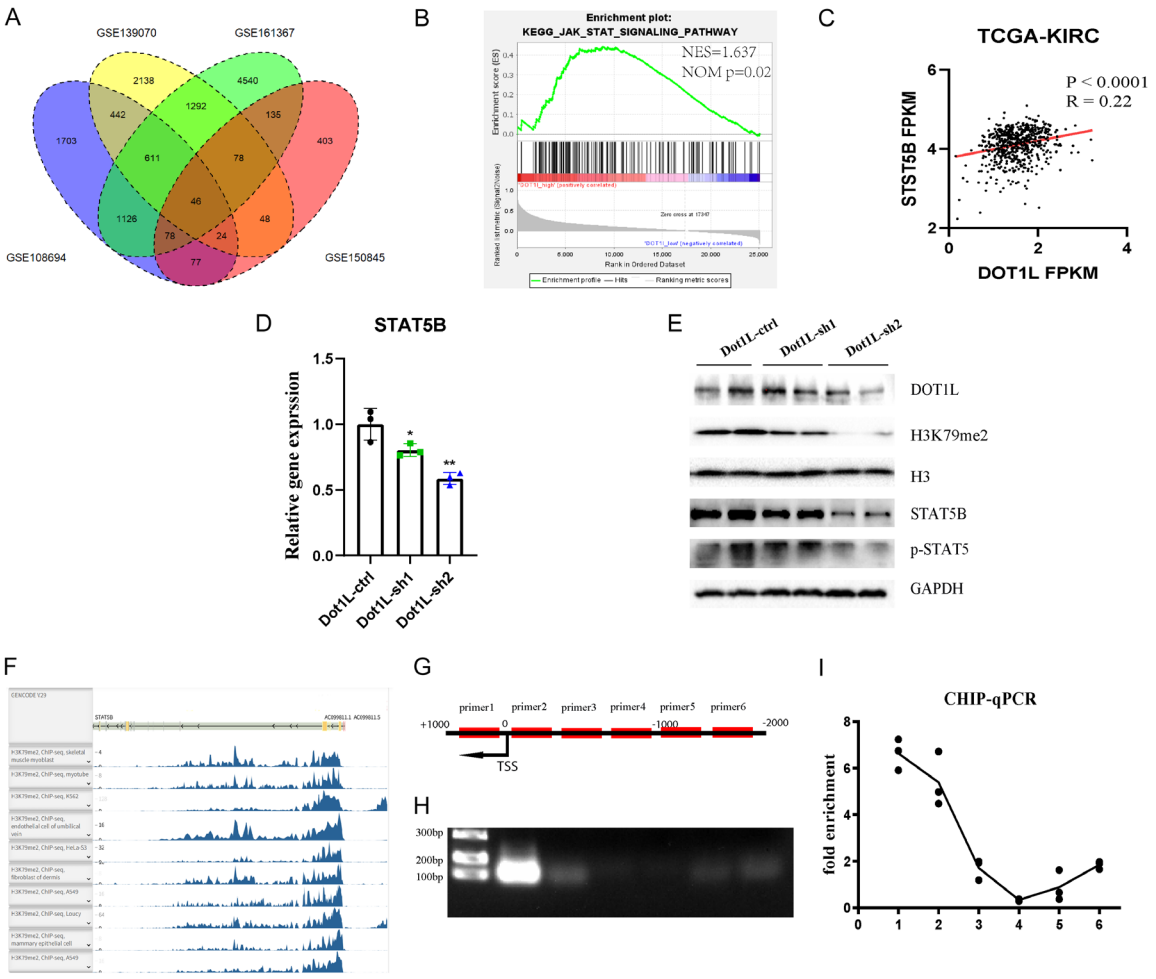

Figure 5. DOT1L silencing demethylates H3K79 and downregulates the transcription of STAT5B. A. A Venn diagram was utilized to identify coexpressed DEGs. B. GSEA showed that DOT1L was closely linked to the KEGG pathway JAK-STAT SIGNALING. C. Pearson correlation between DOT1L and STAT5B expression in KIRC from GEPIA. D. The mRNA level of STAT5B was measured by qPCR in DOT1L knockdown 786-O cells. E. The DOT1L, H3K79me2, STAT5B and p-STAT5 protein levels were measured by Western blotting in DOT1L knockdown 786-O cells. F. ChIP-seq of H3K-79me2 in the ENCODE database showing occupancy on STAT5B promoter in different human cancer cell lines. G. ChIP primer region for human STAT5B. H, I. The ChIP assay showed H3K79me2 occupancy on the STAT5B promoter in 786-O cells by agarose gel electrophoresis and qPCR.

Table 7. Identification of DEGs in four GEO Datasets

Gene Name
BHLHE40 UNC93B1 IGFBP4 ITGB1 GEM PLAC8 CMPK2 MOV10 IFIT1 IGF1R USP18 PRKCE DCAF12 RSAD2 FAM129A TNFSF10 PRNP GNAQ SGK1 CDR2 RNF144A CD44 EGR1 TMEM154 PRR11 MYD88 STAT5B CERCAM ITGA1 DUSP5 MX2 TPX2 ZC3H8 SMAD3 MX1 HERC6 ANXA4 STX1A NUF2 SERPINB9 TOP2A GBP2 IFI30 SH3BP1 SLC37A4 LRP5

decreased in 786-O cells after DOT1L knockdown (**Figure 5D**, **5E**). In addition, the level of H3K79me2 was decreased in response to DOT1L knockdown. DOT1L knockdown induced decreases in both the total STAT5B and p-STAT5 protein levels (**Figure 5E**). Then, to determine whether STAT5B is a direct target of H3K79me2, we performed a ChIP assay. ChIP-seq data from the ENCODE database showed a substantial abundance of H3K79me2 in the key regulatory regions of the STAT5B promoter in human cancer cell lines (**Figure 5F**). Moreover, the ChIP assay showed a high H3K79me2 abundance in the STAT5B promoter (**Figure 5G-I**). Thus,

H3K79me2 directly regulates STAT5B transcription in RCC.

Overexpression of STAT5B partly reverses the suppressive effects of DOT1L knockdown on renal cancer cells

In view of the better effect of DOT1L-sh2 on DOT1L knockdown in 786-O cells, we next explored whether overexpression of STAT5B can alter the inhibitory effects of DOT1L knockdown on renal cancer cells. To overexpress STAT5B in the 786-O cell line, we inserted the CDS domain of STAT5B into the expression vector pEGFP-N1 to generate the pEGFP-N1/STAT5B plasmid. Next, we transfected the pEGFP-N1/STAT5B plasmid into 786-O cells, and after stringent selection in the presence of the antibiotic G418, a clear green fluorescence signal was observed in 786-O cells transfected with either the pEGFP-N1/STAT5B vector (oeSTAT5B) or pEGFP-N1 (sham) vector (**Figure 6A**). There was no difference in the intensity between the DOT1L-sh2+sham group and the sh2+oe group.

To assess whether overexpression of STAT5B via the pEGFP-N1/STAT5B vector or DOT1L knockdown (DOT1L-sh2) was successful in 786-O cells, qPCR and Western blot analyses were performed to verify the expression of STAT5B in 786-O cells. The total STAT5B and p-STAT5 levels were increased after overexpression of STAT5B in 786-O cells (**Figure 6B**, **6C**). The CCK8 assay showed that overexpression of STAT5B in DOT1L knockdown (DOT1L-sh2) 786-O cells (DOT1L-sh2+STAT5B-OE) significantly promoted cell proliferation compared to that in DOT1L-sh2+STAT5B-sham or DOT1L-sh2 786-O cells (**Figure 6D**). Cell cycle analysis by flow cytometry showed that DOT1L-sh2+STAT5B-OE promoted cell cycle progression in these 786-O cells compared with DOT1L-sh2+STAT5B-sham 786-O cells (**Figure 6E**). Simultaneously, we found that the CDK6 protein level was increased and the p21 protein level was decreased in STAT5B-OE cells (**Figure 6F**). Together, these findings indicated that overexpression of STAT5B effectively reversed the suppressive effects of DOT1L knockdown on renal cancer cells.

CDK6 acts as a downstream effector of STAT5B to mediate inhibition of the cell cycle

We found that the expression of CDK6 was consistent with that of STAT5B. Thus, we investigated the influence of STAT5B on CDK6 expression in 786-O cells by qPCR and Western blotting. Overexpression of STAT5B increased the CDK6 mRNA and protein levels (**Figure 7A**, **7B**). By inspecting the sequences of the promoter of CDK6 using the JASPAR database, we identified the STAT5B binding sites within the promoter region (**Figure 7C**). We then transiently cotransfected the STAT5B overexpression plasmid with the CDK6 promoter reporter plasmid into 786-O cells and found that luciferase activity was upregulated by STAT5B overexpression (**Figure 7D**). Moreover, the ChIP assay showed that STAT5B bound to the promoter of CDK6 (**Figure 7E**, **7F**). Collectively, these results suggest that STAT5B binds directly to the promoter of CDK6 and activates CDK6 transcription.

Discussion

Histone lysine methylation is a critical epigenetic regulatory feature with important functions in many cancer-related events. DOT1L is a chromatin modifier that functions as the H3K79 methyltransferase. DOT1L has been found to be associated with several cancers. In acute leukemia, DOT1L has been shown to be necessary for the development of leukemia in patients with MLL translocations [22]. Pinometostat, a small molecule DOT1L inhibitor, has entered clinical trials [23]. In prostate cancer, DOT1L inhibition concurrently suppresses AR and MYC protein expression, resulting in impaired prostate tumorigenicity [24]. In colorectal cancer, DOT1L inhibition causes cell cycle arrest by epigenetically altering the expression of c-Myc [12]. In ovarian cancer, DOT1L stimulates protumorigenic metabolic pathways, inhibits apoptosis, and promotes tumor growth [25].

A previous study showed that higher DOT1L expression indicated a poor clinical prognosis in patients [15]. However, the detailed mechanism of DOT1L in ccRCC is not known. In this study, we found that DOT1L is highly expressed in RCC and is predictive of poor prognosis. We showed that SGC0946, a DOT1L inhibitor, inhibits the growth and invasion of renal cancer cells. Similar results were observed in renal cancer cells transduced with DOT1L shRNA. This evidence suggests that DOT1L might be a novel therapeutic target in RCC.

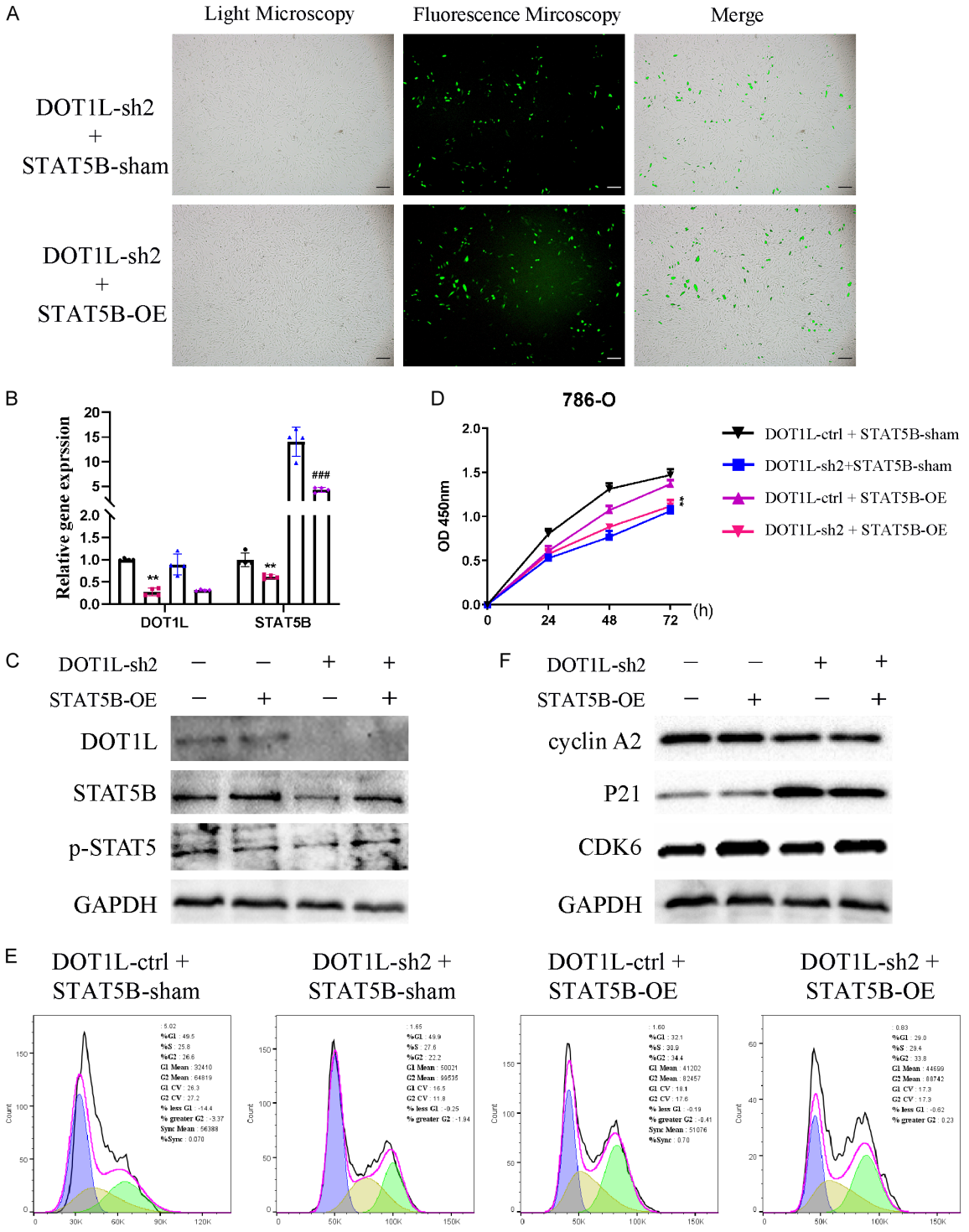

Figure 6. Overexpression of STAT5B partially rescues DOT1L silencing-induced cell proliferation inhibition and cell cycle arrest. A. Assessment of the DNA transfection efficiency after incubation with the pEGFP-N1/STAT5B vector (oeSTAT5B) or the pEGFP-N1 (sham) vector in 786-O cells with sh2-mediated DOT1L knockdown at the 24 h time point. B. DOT1L and STAT5B mRNA expression was measured by using qPCR in 786-O cells after DOT1L silencing and STAT5B overexpression. C. DOT1L, STAT5B and p-STAT5 protein levels were measured by Western blotting in 786-O cells after DOT1L knockdown and STAT5B overexpression. D. The cell growth curve was constructed with CCK8 assay data in 786-O cells after DOT1L knockdown and STAT5B overexpression. Both the sh2 and sh2+sham groups were used as the vector controls for STAT5B overexpression at the 0/24/48/72 h time points. E. The cell cycle was analyzed by flow cytometry in 786-O cells with DOT1L knockdown and STAT5B restoration. F. Cyclin A2, P21, and CDK6 protein expression was measured by Western blotting in 786-O cells after DOT1L knockdown and STAT5B overexpression.

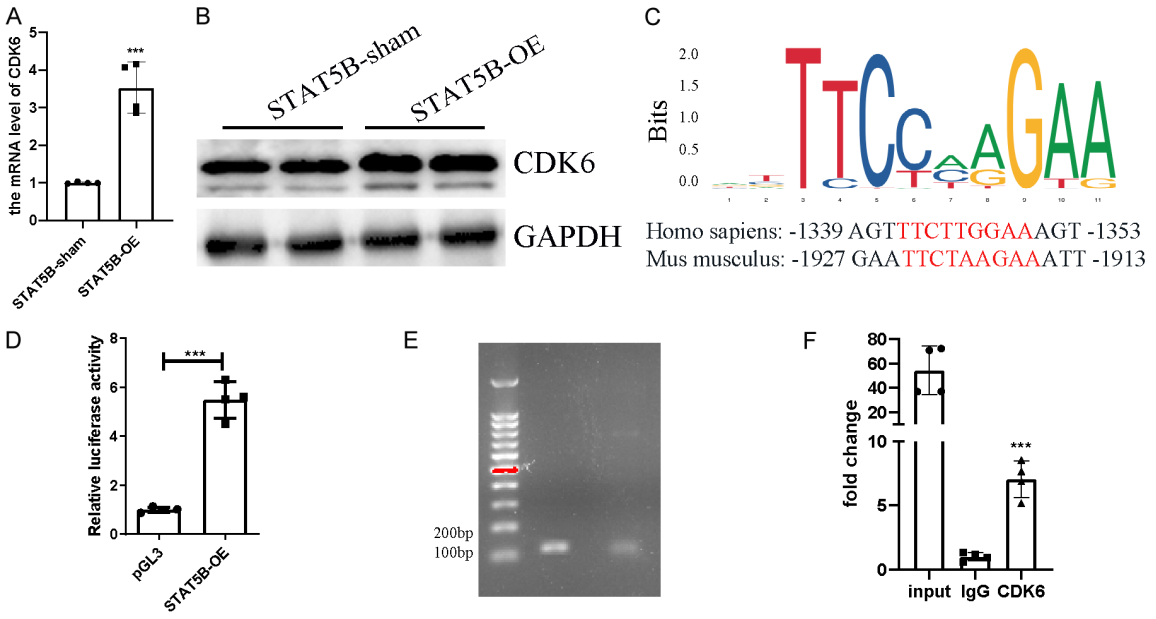

Figure 7. STAT5B binds to the CDK6 promoter and activates CDK6 transcription. A, B. The mRNA and protein expression levels of CDK6 in renal cancer cells after overexpression of STAT5B were measured by qPCR and Western blotting. C. Schematic diagram showing the STAT5B binding sites in the CDK6 promoter region predicted by JASPAR. D. The relative luciferase activity of the CDK6 promoter reporter in transiently transfected 786-O cells were examined by a dual-luciferase reporter assay. E, F. The binding region of STAT5B in the promoter of CDK6 was identified by a ChIP assay in 786-O cells.

STAT5B is a crucial node in the transcriptional activation chain following cytokine or kinase activity in many different kinds of cancers [26, 27]. STAT5B inhibition in cancer cells leads to attenuated growth, apoptosis and invasion [28-31]. STAT5B suppression inhibits the proliferation of human glioblastoma multiforme cells, causes G1 arrest, and decreases tumor cell invasion [32]. Prior research demonstrated that DOT1L inhibition decreases the levels of H3K79me2 and STAT5B, leading to T-cell death and dysfunction [18]. Here, we showed that DOT1L expression was positively associated with STAT5B expression in renal cancer cells and that H3K79me2 was enriched in the STAT5B promoter in 786-O cells.

In this study, we found that either inhibiting or silencing DOT1L significantly induced S-phase arrest. Consistent with previous findings, ovarian cancer cells and colorectal cancer cells with DOT1L silencing undergo G1/S arrest [11, 12]. Our study indicated that cell cycle-related proteins responded to DOTL silencing: for example, the levels of cyclin A2, cyclin D2, CDK2, CDK4, and CDK6 were significantly decreased after DOT1L silencing, while those of p21 and p53 expression were significantly increased. After overexpression of STAT5B, the CDK6 protein level was increased and the p21 protein level was decreased. Then, we demonstrated that STAT5B bound to the CDK6 promoter region and activated CDK6 transcription, consequently promoting CDK6 protein expression and accelerating the cell cycle in renal cancer cells. Collectively, these results indicated that STAT5B accelerated cell cycle progression by regulating DOT1L expression (**Figure 8**).

SGC0946 is a highly selective DOT1L methyltransferase inhibitor [33]. Previously, SGC0946 was found to suppress H3K79 methylation and proliferation in neuroblastoma cells [34] and to contribute to inhibiting metastasis and improving clinical responses in lung cancer [35]. We also discovered that SGC0946 inhibited the proliferation and invasion of renal cancer cells. Our data showed that SGC0946 has an anticancer effect in RCC and might be a useful therapeutic agent for RCC.

Conclusion

Our study showed that either silencing or inhibition of DOT1L suppresses cell proliferation,

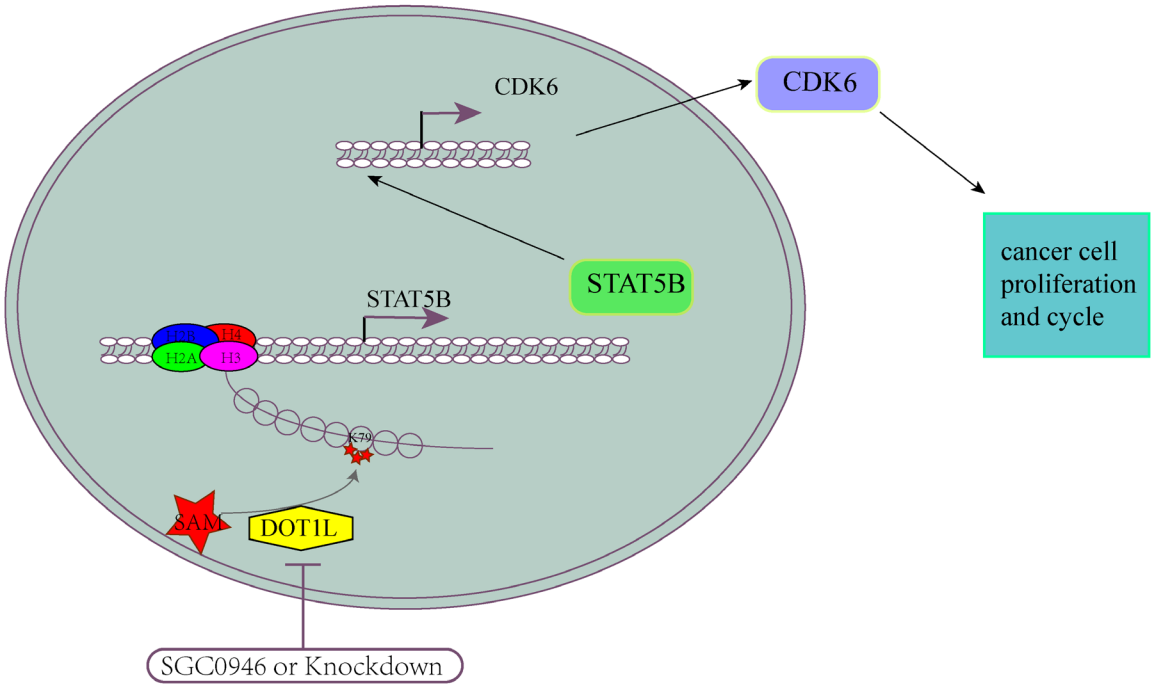

Figure 8. Schematic model showing that the DOT1L-STAT5B-CDK6 axis regulates the proliferation and invasion of renal cancer cells.

induces S-phase arrest, and blocks tumor invasion via epigenetic downregulation of STAT5B expression in RCC. Targeting DOT1L might thus be a therapeutic strategy for RCC.

Acknowledgements

This research was supported by grants from National Natural Science Foundation of China (No. 81972408), the key research and development program of Hubei Province (No. 2020BCB051), and the Fundamental Research Funds for the Central Universities (2042021kf0105).

Disclosure of conflict of interest

None.

Address correspondence to: Juncheng Hu and Xiuheng Liu, Department of Urology, Renmin Hospital of Wuhan University, Wuhan 430060, Hubei, PR China. E-mail: hujc@whu.edu.cn (JCH); drliuxh@hotmail.com (XHL)

References

[1] Siegel RL, Miller KD and Jemal A. Cancer statistics, 2019. CA Cancer J Clin 2019; 69: 7-34.

[2] Brugarolas J. Molecular genetics of clear-cell renal cell carcinoma. J Clin Oncol 2014; 32: 1968-1976.

[3] Capitanio U, Cloutier V, Zini L, Isbarn H, Jeldres C, Shariat SF, Perrotte P, Antebi E, Patard JJ, Montorsi F and Karakiewicz PI. A critical assessment of the prognostic value of clear cell, papillary and chromophobe histological subtypes in renal cell carcinoma: a population-based study. BJU Int 2009; 103: 1496-1500.

[4] Escudier B, Porta C, Schmidinger M, Rioux-Leclercq N, Bex A, Khoo V, Gruenvald V and Horwich A; ESMO Guidelines Committee. Renal cell carcinoma: ESMO clinical practice guidelines for diagnosis, treatment and follow-up. Ann Oncol 2016; 27: v58-v68.

[5] Bannister AJ and Kouzarides T. Regulation of chromatin by histone modifications. Cell Res 2011; 21: 381-395.

[6] Audia JE and Campbell RM. Histone modifications and cancer. Cold Spring Harb Perspect Biol 2016; 8: a019521.

[7] Wood K, Tellier M and Murphy S. DOT1L and H3K79 methylation in transcription and genomic stability. Biomolecules 2018; 8: 11.

[8] Grigsby SM, Friedman A, Chase J, Waas B, Ropa J, Serio J, Shen C, Muntean AG, Maillard I and Nikolovska-Coleska Z. Elucidating the importance of DOT1L recruitment in MLL-AF9 leukemia and hematopoiesis. Cancers (Basel) 2021; 13: 642.

[9] Bernt KM, Zhu N, Sinha AU, Vempati S, Faber J, Krivtsov AV, Feng Z, Punt N, Daigle A, Bullinger L, Pollock RM, Richon VM, Kung AL and Armstrong SA. MLL-rearranged leukemia is dependent on aberrant H3K79 methylation by DOT1L. Cancer Cell 2011; 20: 66-78.

[10] Byun WS, Kim WK, Han HJ, Chung HJ, Jang K, Kim HS, Kim S, Kim D, Bae ES, Park S, Lee J, Park HG and Lee SK. Targeting histone methyltransferase DOT1L by a novel Psammaplin A analog inhibits growth and metastasis of triple-negative breast cancer. Mol Ther Oncolytics 2019; 15: 140-152.

[11] Zhang X, Liu D, Li M, Cao C, Wan D, Xi B, Li W, Tan J, Wang J, Wu Z, Ma D and Gao Q. Prognostic and therapeutic value of disruptor of telomeric silencing-1-like (DOT1L) expression in patients with ovarian cancer. J Hematol Oncol 2017; 10: 29.

[12] Yang L, Lei Q, Li L, Yang J, Dong Z and Cui H. Silencing or inhibition of H3K79 methyltransferase DOT1L induces cell cycle arrest by epigenetically modulating c-Myc expression in colorectal cancer. Clin Epigenetics 2019; 11: 199.

[13] Vatapalli R, Sagar V, Rodriguez Y, Zhao JC, Unno K, Pamarthy S, Lysy B, Anker J, Han H, Yoo YA, Truica M, Chalmers ZR, Giles F, Yu J, Chakravarti D, Carneiro B and Abdulkadir SA. Histone methyltransferase DOT1L coordinates AR and MYC stability in prostate cancer. Nat Commun 2020; 11: 4153.

[14] Song Z, Wei Z, Wang Q, Zhang X, Tao X, Wu N, Liu X and Qian J. The role of DOT1L in the proliferation and prognosis of gastric cancer. Biosci Rep 2020; 40: BSR20193515.

[15] Qu Y, Liu L, Wang J, Xi W, Xia Y, Bai Q, Xiong Y, Long Q, Xu J and Guo J. Dot1l expression predicts adverse postoperative prognosis of patients with clear-cell renal cell carcinoma. Oncotarget 2016; 7: 84775-84784.

[16] Wong M, Tee AEL, Milazzo G, Bell JL, Poulos RC, Atmadibrata B, Sun Y, Jing D, Ho N, Ling D, Liu PY, Zhang XD, Huttelmaier S, Wong JWH, Wang J, Polly P, Perini G, Scarlett CJ and Liu T. The histone methyltransferase DOT1L promotes neuroblastoma by regulating gene transcription. Cancer Res 2017; 77: 2522-2533.

[17] Pan F, Wang Q, Li S, Huang R, Wang X, Liao X, Mo H, Zhang L and Zhou X. Prognostic value of key genes of the JAK-STAT signaling pathway in patients with cutaneous melanoma. Oncol Lett 2020; 19: 1928-1946.

[18] Bian Y, Li W, Kremer DM, Sajjakulnukit P, Li S, Crespo J, Nwosu ZC, Zhang L, Czerwonka A, Pawlowska A, Xia H, Li J, Liao P, Yu J, Vatan L, Szeliga W, Wei S, Grove S, Liu JR, McLean K, Cieslik M, Chinnaiyan AM, Zgodzinski W, Wallner G, Wertel I, Okla K, Kryczek I, Lyssiotis CA and Zou W. Cancer SLC43A2 alters T cell methionine metabolism and histone methylation. Nature 2020; 585: 277-282.

[19] Lin H, Cheng K, Kubota H, Lan Y, Riedel SS, Kakiuchi K, Sasaki K, Bernt KM, Bartolomei MS, Luo M and Wang PJ. Histone methyltransferase DOT1L is essential for self-renewal of germline stem cells. Genes Dev 2022; 36: 752-763.

[20] Schubeler D, MacAlpine DM, Scalzo D, Wirbelauer C, Kooperberg C, van Leeuwen F, Gottschling DE, O'Neill LP, Turner BM, Delrow J, Bell SP and Groudine M. The histone modification pattern of active genes revealed through genome-wide chromatin analysis of a higher eukaryote. Genes Dev 2004; 18: 1263-1271.

[21] Zhou X, Chen H, Li J, Shi Y, Zhuang S and Liu N. The role and mechanism of lysine methyltransferase and arginine methyltransferase in kidney diseases. Front Pharmacol 2022; 13: 885527.

[22] Nguyen AT, Taranova O, He J and Zhang Y. DOT1L, the H3K79 methyltransferase, is required for MLL-AF9-mediated leukemogenesis. Blood 2011; 117: 6912-6922.

[23] Stein EM, Garcia-Manero G, Rizzieri DA, Tibes R, Berdeja JG, Savona MR, Jongen-Lavrenic M, Altman JK, Thomson B, Blakemore SJ, Daigle SR, Waters NJ, Suttle AB, Clawson A, Pollock R, Krivtsov A, Armstrong SA, DiMartino J, Hedrick E, Lowenberg B and Tallman MS. The DOT1L inhibitor pinometostat reduces H3K79 methylation and has modest clinical activity in adult acute leukemia. Blood 2018; 131: 2661-2669.

[24] Vatapalli R, Sagar V, Rodriguez Y, Zhao JC, Unno K, Pamarthy S, Lysy B, Anker J, Han H, Yoo YA, Truica M, Chalmers ZR, Giles F, Yu J, Chakravarti D, Carneiro B and Abdulkadir SA. Histone methyltransferase DOT1L coordinates AR and MYC stability in prostate cancer. Nat Commun 2020; 11: 4153.

[25] Chava S, Bugide S, Edwards YJK and Gupta R. Disruptor of telomeric silencing 1-like promotes ovarian cancer tumor growth by stimulating pro-tumorigenic metabolic pathways and blocking apoptosis. Oncogenesis 2021; 10: 48.

[26] Orlova A, Wagner C, de Araujo ED, Bajusz D, Neubauer HA, Herling M, Gunning PT, Keseru GM and Moriggl R. Direct targeting options for STAT3 and STAT5 in cancer. Cancers (Basel) 2019; 11: 1930.

[27] Verhoeven Y, Tilborghs S, Jacobs J, De Waele J, Quatannens D, Deben C, Prenen H, Pauwels P, Trinh XB, Wouters A, Smits ELJ, Lardon F and van Dam PA. The potential and controversy of

targeting STAT family members in cancer. Semin Cancer Biol 2020; 60: 41-56.
[28] Sumiyoshi H, Matsushita A, Nakamura Y, Matsuda Y, Ishiwata T, Naito Z and Uchida E. Suppression of STAT5b in pancreatic cancer cells leads to attenuated gemcitabine chemoresistance, adhesion and invasion. Oncol Rep 2016; 35: 3216-3226.
[29] Subramaniam D, Angulo P, Ponnurangam S, Dandawate P, Ramamoorthy P, Srinivasan P, Iwakuma T, Weir SJ, Chastain K and Anant S. Suppressing STAT5 signaling affects osteosarcoma growth and stemness. Cell Death Dis 2020; 11: 149.
[30] S P N, Darvin P, Yoo YB, Joung YH, Kang DY, Kim DN, Hwang TS, Kim SY, Kim WS, Lee HK, Cho BW, Kim HS, Park KD, Park JH, Chang SH and Yang YM. The combination of methylsulfonylmethane and tamoxifen inhibits the Jak2/STAT5b pathway and synergistically inhibits tumor growth and metastasis in ER-positive breast cancer xenografts. BMC Cancer 2015; 15: 474.
[31] Moyama C, Fujita M, Ando S, Taniguchi K, Ii H, Tanigawa S, Hashimoto N and Nakata S. Stat5b inhibition blocks proliferation and tumorigenicity of glioblastoma stem cells derived from a de novo murine brain cancer model. Am J Cancer Res 2022; 12: 1129-1142.
[32] Liang QC, Xiong H, Zhao ZW, Jia D, Li WX, Qin HZ, Deng JP, Gao L, Zhang H and Gao GD. Inhibition of transcription factor STAT5b suppresses proliferation, induces G1 cell cycle arrest and reduces tumor cell invasion in human glioblastoma multiforme cells. Cancer Lett 2009; 273: 164-171.
[33] Yu W, Chory EJ, Wernimont AK, Tempel W, Scopton A, Federation A, Marineau JJ, Qi J, Barsyte-Lovejoy D, Yi J, Marcellus R, Iacob RE, Engen JR, Griffin C, Aman A, Wienholds E, Li F, Pineda J, Estiu G, Shatseva T, Hajian T, Al-Awar R, Dick JE, Vedadi M, Brown PJ, Arrowsmith CH, Bradner JE and Schapira M. Catalytic site remodelling of the DOT1L methyltransferase by selective inhibitors. Nat Commun 2012; 3: 1288.
[34] Wong M, Tee AEL, Milazzo G, Bell JL, Poulos RC, Atmadibrata B, Sun Y, Jing D, Ho N, Ling D, Liu PY, Zhang XD, Huttelmaier S, Wong JWH, Wang J, Polly P, Perini G, Scarlett CJ and Liu T. The histone methyltransferase DOT1L promotes neuroblastoma by regulating gene transcription. Cancer Res 2017; 77: 2522-2533.
[35] Evanno E, Godet J, Piccirilli N, Guilhot J, Milin S, Gombert JM, Fouchaq B and Roche J. Trimethylation of H3K79 is decreased in TGF-beta1-induced epithelial-to-mesenchymal transition in lung cancer. Clin Epigenetics 2017; 9: 80.